

1 mrangr: An R package for mechanistic simulation of metacommunities

2 Katarzyna Markowska ^{*1}, Michał Wawrzynowicz¹, Lechośław Kuczyński¹

3 ¹ Population Ecology Lab, Faculty of Biology, Adam Mickiewicz University, Uniwersytetu
4 Poznańskiego 6, 61-614 Poznań, Poland

5 * Corresponding author: katarzyna.markowska@amu.edu.pl

6 ORCID's

7 Katarzyna Markowska 0000-0001-5646-4611

8 Michał Wawrzynowicz 0009-0001-3729-3439

9 Lechośław Kuczyński 0000-0003-3498-5445

10 Abstract

11 Metacommunity theory unifies ecology by integrating local biotic interactions with regional
12 dispersal and environmental filtering. However, testing theoretical predictions against empirical
13 data remains challenging due to the difficulty of disentangling these processes in nature and the
14 confounding effects of imperfect detection. Here, we introduce `mrangr`, an R package designed
15 for the mechanistic, spatially explicit simulation of multispecies communities. Unlike correlative
16 approaches, `mrangr` strictly distinguishes between the fundamental niche (determined by
17 abiotic carrying capacity) and the realised niche (an emergent property of biotic interactions). The
18 package implements a generalized Lotka-Volterra framework on a lattice grid (via the `terra`
19 ecosystem), allowing users to simulate diverse interaction types — including competition,
20 predation, and facilitation — alongside species-specific dispersal kernels. A defining feature is the
21 'virtual ecologist' module, which samples the simulated ground truth with user-defined
22 observation errors and sampling designs, thereby mimicking the constraints of real-world

23 biodiversity surveys. We demonstrate the package's capabilities through three case studies:
24 (i) quantifying the scale-dependent effects of dispersal on α , β , and γ diversity, (ii) testing the
25 conditions under which the competition-colonization trade-off promotes coexistence in the
26 presence of fitness inequalities, and (iii) assessing the recoverability of fundamental niches from
27 imperfect observational data constrained by biotic interactions. By providing a flexible platform
28 to generate synthetic spatial data with known underlying mechanisms, `mrangr` enables
29 researchers to benchmark complex statistical models (e.g. JSDMs), assess sampling strategies, and
30 rigorously test hypotheses at the interface of theoretical and empirical macroecology.

31

32 **Key-words:** metacommunity dynamics, fundamental and realized niche, community assembly,
33 process-based modelling, virtual ecologist, spatially explicit

34 **Running Head:** Mechanistic metacommunity simulation in R

35 1. Introduction

36 One of the key goals of ecology is to understand the mechanisms generating and maintaining
37 biodiversity. Traditionally, theory separated these mechanisms by spatial scale: regional frameworks
38 emphasized ecological drift, selection, speciation, and dispersal (Vellend, 2016), whereas local models
39 focused on competitive coexistence (Chesson, 2000), and priority effects (Adler et al., 2007; Ke &
40 Letten, 2018). Metacommunity theory (M. A. Leibold et al., 2004, 2017) unifies these perspectives by
41 identifying three spatially explicit mechanisms that operate across scales: density-independent
42 responses to abiotic conditions, density-dependent biotic interactions, and dispersal (Thompson et
43 al., 2020). While explicitly integrating these mechanisms is essential for understanding biodiversity
44 patterns, a central debate in macroecology remains the extent to which local biotic interactions leave
45 a signature at regional and continental scales (Araújo & Rozenfeld, 2014). Testing such spatial scaling
46 theories is currently hindered by a critical limitation in many existing metacommunity tools: the
47 conflation of the fundamental and realized niche. Frequently, simulators rely on input suitability maps
48 that implicitly incorporate biotic constraints, rendering it impossible to disentangle environmental
49 filtering from community processes. To overcome this, a mechanistic framework must strictly define
50 the fundamental niche as a measure of environmental potential, allowing the realized niche to emerge
51 purely as a dynamic property of biotic interactions and dispersal.

52 The R programming environment has become the standard for macroecological research, offering
53 robust tools to evaluate empirical metacommunity structure from static distribution matrices (e.g.,
54 Dallas, 2014). However, although these analytical packages excel at quantifying spatial patterns, they
55 cannot simulate the underlying mechanistic processes that generate them. To move from correlative
56 pattern description to process-based hypothesis testing, researchers require generative models
57 capable of explicitly simulating community assembly over time and space. However, despite the need
58 for mechanistic clarity, the current landscape of process-based metacommunity simulators – namely
59 `gen3sis` (Hagen et al., 2021) and `metaIBM` (Lin et al., 2024) - often necessitates trade-offs. While

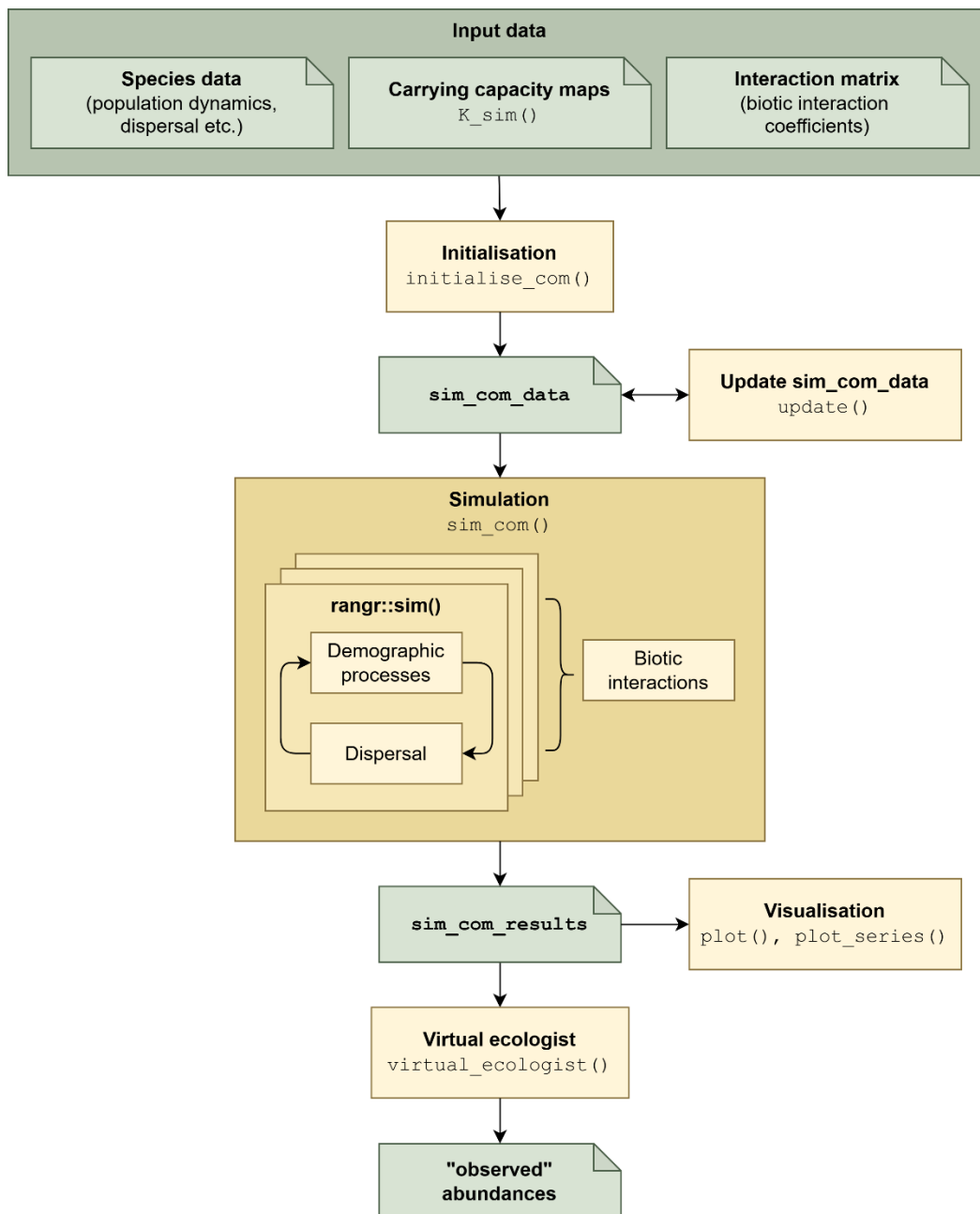
60 these frameworks share a core principle of coupling dispersal and density-dependent regulation, they
61 implement interspecific regulation indirectly by the magnitude of fundamental niche overlap. This
62 reliance on overlap prevents the explicit modelling of metacommunities with asymmetric (e.g.
63 predation) or positive (e.g. facilitation) interactions, effectively locking the simulation into the
64 "conflated niche" paradigm. Conversely, `metaRange` (Fallert et al., 2025) provides a programming
65 environment in which multiple processes, including all types of biotic interactions, can be modelled
66 flexibly; yet users must code these functionalities themselves. Consequently, no off-the-shelf tool is
67 currently capable of simulating metacommunities with flexible, asymmetric biotic interactions while
68 maintaining a strict separation between abiotic and biotic drivers.

69 To address this gap, we have developed `mrangr`: an R package for flexible, mechanistic
70 metacommunity simulation in which dispersal processes, demographic rates and biotic interaction
71 coefficients can be explicitly parametrised. Built as a multi-species extension of the `rangr` package
72 (Markowska et al., 2025), `mrangr` inherits that tool's accessible parameterisation of population
73 dynamics, dispersal, and virtual ecology. By representing species relationships through an asymmetric
74 interaction matrix, it enables the simulation of diverse biotic interactions - including competition,
75 facilitation, and predation - within a spatially explicit virtual environment. Moreover, by defining the
76 fundamental niche strictly through user-supplied carrying capacity maps, the package allows the
77 realized niche to emerge dynamically. This separation enables researchers to quantify the "biotic
78 deficit" - the specific loss of range or abundance attributable solely to biotic interactions - by
79 comparing the input carrying capacity maps against the simulated equilibrium state.

80 2. Package overview

81 The core architecture of `mrangr` is designed to mechanistically decouple the fundamental niche from
82 the realized niche (Figure 1). Users define the environmental potential for each species via spatially
83 explicit carrying capacity maps (K) and intrinsic growth rates (r), while biotic constraints are governed

84 by a user-supplied asymmetric interaction matrix (a). Consequently, the realized metacommunity
85 emerges dynamically from the interplay of species-specific demography, dispersal constraints, and
86 pairwise interactions. To bridge the gap between these theoretical mechanisms and empirical reality,
87 the package includes a 'virtual ecologist' module that replicates both observation error and the specific
88 sampling designs of biological surveys. Crucially, this module generates outputs that mimic the
89 structure of empirical monitoring data, such as sparse spatiotemporal records rather than complete
90 grids. This structural fidelity allows researchers to feed simulated datasets directly into standard
91 analytical pipelines (e.g., SDMs or occupancy models), providing a rigorous platform for benchmarking
92 statistical methods against a known ground truth. A comprehensive overview of the supported
93 biological and observational processes is provided in Table 1.



94

95 Figure 1. Conceptual framework and operational workflow of the `mrangr` package. The schematic
 96 illustrates the mechanistic decoupling of drivers: the fundamental niche is strictly defined by input
 97 carrying capacity maps, while the realized niche emerges dynamically from the integration of biotic
 98 interactions, demographic rates, and dispersal. The workflow progresses from initialization to the
 99 'virtual ecologist' module, which simulates observational errors. Green rectangles represent data
 100 objects (inputs and state variables), while yellow rectangles represent the package's core functions
 101 governing metapopulation dynamics and sampling.

102 Table 1. Overview of the `mrangr` framework, distinguishing between the ecological state processes
 103 (mechanisms generating the true abundance) and the observation model (mechanisms generating
 104 survey data).

Simulation Component	Impact	Implementation in <code>mrangr</code>
PROCESS MODEL		
Abiotic constraints (Fundamental niche)	Defines the potential range and maximum abundance of a species based solely on environmental physiology, ignoring other species.	Users supply carrying capacity maps (K), either as static rasters or generated dynamically via <code>K_sim()</code> based on environmental variables.
Biotic filtering (Realized niche)	Modifies the fundamental niche by reducing abundance (competition, predation) or expanding it (facilitation), creating the realized distribution.	The interaction matrix (a) defines pairwise coefficients. The simulation solves for abundance at each time step, allowing the realized niche to emerge dynamically from the K maps and matrix a .
Dispersal	Regulates connectivity. Low rates cause dispersal limitation, preventing species from reaching suitable patches. High rates drive mass effects (source-sink dynamics) and rescue effects.	Users control the spread via the <code>kernel_fun</code> parameter in <code>initialise_com()</code> . This allows for modelling constrained diffusion (limitation) or fat-tailed distributions (long distance dispersal) to simulate different isolation scenarios.
Ecological drift	Stochastic changes in abundance, dominant in small populations.	Demographic stochasticity is inherent to the simulation. Additional noise can be introduced into demographic rates or environmental layers using <code>initialise_com()</code> or <code>update()</code> functions.
OBSERVATION MODEL		
Observation process	Distorts biological patterns through sampling bias and imperfect detection. Essential for validating analytical methods against "known" truths.	The <code>virtual_ecologist()</code> function samples the simulated metacommunity. Users can specify sampling designs (e.g., random, systematic) and detection probability distributions (e.g., <code>obs_error</code>) to generate realistic "observed" datasets.

105 3. Key features of the package

106 `mrangr` inherits the core population dynamics of `rangr`, including spatially explicit growth models,
107 flexible dispersal kernels, and non-monotonic regulation (e.g., Allee effects). As these fundamental
108 mechanisms are detailed in Markowska *et al.* (2025), we focus here on the novel functionalities
109 emerging from their integration into a multi-species context.

110 3.1. Interspecific regulation

111 Central to `mrangr` is a generalized interaction matrix that enables the simulation of diverse
112 community dynamics. By parameterising both positive and negative coefficients in an
113 asymmetric matrix (a), users can represent a full spectrum of ecological interactions, including
114 competition, facilitation, and predation.

115 Biotic interactions are modelled via a square numeric matrix where each element a_{ij}
116 represents the *per-capita* interaction strength of species j on species i . Mechanistically, this
117 coefficient defines the change in the carrying capacity of species i caused by a single individual
118 of species j . Consequently, the realized niche is calculated dynamically: at each time step, the
119 effective carrying capacity of a focal species is derived by modifying its fundamental niche
120 (K_{fund}) by the net biotic influence of the community.

121 Formally, the effective carrying capacity for species i at time t in a given cell is calculated as:

$$122 \quad K_{i,t} = \max \left(K_{i,fund} + \sum_{j=1}^S (a_{i,j} \cdot N_{j,t-1}), 0 \right)$$

123 where S is the total number of species, $N_{j,t-1}$ is the abundance of species j at the previous
124 time step, and the $\max(\dots, 0)$ function ensures that carrying capacity remains non-negative.

125 This formulation represents a specific implementation of the Lotka-Volterra framework where
126 interactions expand or contract the available niche space (K) rather than acting directly on
127 intrinsic growth rates (r).

128 **3.2. Low entry level**

129 The package is designed to minimize technical complexity, requiring only two primary
130 functions to execute a complete simulation. First, a community object is established using the
131 `initialise_com()`, which integrates spatial carrying capacity maps (K), the biotic
132 interaction matrix (a) and species-specific life-history parameters. Subsequently, the
133 `sim_com()` function executes the spatially explicit simulation. This streamlined workflow
134 reduces the programming workload, allowing ecologists to study complex feedback loops and
135 metacommunity dynamics without having to create custom simulation engines.

136 **3.3. Invasion dynamics**

137 The package offers specialised functionality to simulate species invasions. Users can designate
138 specific species as invaders and schedule their introduction at defined time steps, rather than
139 initializing them at the start of the simulation. This temporal flexibility enables the mechanistic
140 investigation of invasion success. It allows researchers to explore how community
141 composition, biotic resistance and arrival timing shape the settlement of new species within
142 established metacommunities.

143 **3.4. Virtual ecologist**

144 A major challenge in spatial ecology is that theoretical models often assume perfect
145 knowledge, whereas empirical data is inherently noisy and incomplete. To bridge this gap,
146 `mrangr` includes a 'virtual ecologist' module designed to replicate the constraints of real-
147 world biological surveys (Zurell et al., 2010). While the simulation inherently generates "true"
148 abundances, the `virtual_ecologist()` function allows users to filter this output
149 through imperfect observation methods. The module supports:

- 150 • Sampling designs: Users can define the sampling intensity (e.g., surveying only 5% of
151 the landscape) and spatial configuration (random vs. systematic sampling).

- 152 • Detection error: It simulates imperfect detection and observation bias by applying
153 error distributions (e.g. Binomial to mimic imperfect detectability or log-Normal to
154 impose observation error on counts) to true abundance data.

155 Building on recent efforts to make virtual species more realistic (Malinowska et al., 2023), this
156 module generates "observed" datasets alongside known, mechanistically derived ground
157 truths. This dual-output framework allows researchers to rigorously benchmark statistical
158 methods (such as species distribution models or occupancy models) and quantify how
159 sampling limitations affect ecological inference (Meynard et al., 2019).

160 3.5. Virtual environment generator

161 To facilitate theoretical investigations, the `K_sim()` function allows for the generation of
162 spatially explicit carrying capacity maps based on spatially autocorrelated Gaussian Random
163 Fields (GRFs). This tool enables users to construct controlled synthetic landscapes by defining
164 both the spatial structure (via the autocorrelation range) and the statistical properties
165 (marginal distributions) of the environment. Furthermore, the function supports the
166 specification of cross-correlations between different landscape layers, allowing researchers to
167 simulate complex niche relationships — such as environmental trade-offs or positive
168 associations — under precise experimental conditions. This offers a versatile framework for
169 testing ecological hypotheses across a range of environmental configurations.

170 3.6. GIS integration

171 Unlike theoretical tools that rely solely on synthetic landscapes, `mrangr` is fully integrated
172 with the `terra` ecosystem, the modern standard for spatial data analysis in R (Hijmans,
173 2026). This interoperability allows users to directly ingest empirical raster data — such as
174 climate layers, land cover maps, or remote sensing outputs — to define simulation arenas. By
175 enabling the use of real-world geographical data as boundary conditions, `mrangr` facilitates

176 the seamless transition from abstract theoretical exploration to data-driven macroecological
177 modelling.

178 3.7. Computational efficiency

179 Spatially explicit simulations are often computationally expensive, particularly when scaling
180 up to large landscapes or high species richness. `mrangr` addresses this by delegating
181 intensive spatial operations to the `terra` package, which is optimized in C++. This allows the
182 package to maintain the flexibility and readability of pure R code while achieving the
183 performance necessary to handle large landscape grids and extensive replication.
184 Furthermore, the package is designed to support parallel execution. As demonstrated in the
185 provided case studies, users can easily distribute replicates across processor cores using
186 standard R parallelization tools (e.g., `parallel`, `pbapply`), making it feasible to conduct
187 extensive sensitivity analyses and robustly estimate parameter uncertainty.

188 4. `mrangr` workflow

189 The `mrangr` package provides a straightforward workflow consisting of 3 main steps.

190 4.1. Environment and community initialisation

191 The workflow begins by defining the simulation arena and the community structure. Users can
192 integrate empirical spatial data by providing `SpatRaster` objects for carrying capacity maps (K),
193 representing species fundamental niches, and initial abundance maps (N_1). Alternatively, for
194 theoretical applications or sensitivity testing, the `K_sim()` function allows users to generate
195 synthetic, spatially autocorrelated carrying capacity landscapes. Concurrently, interspecific
196 dynamics are parameterised via an asymmetric interaction matrix (a), enabling the representation
197 of complex biotic relationships. The `initialise_com()` function integrates the spatial data
198 and interaction parameters into a `sim_com_data` object. At this stage, users define species-

199 specific traits, including intrinsic growth rates (r) and dispersal kernels (`kernel_fun`). This step
200 validates the input maps and community parameters before the simulation begins, while also
201 encapsulating all this data into a single `sim_com_data` object.

202 4.2. Simulation execution

203 Once the system is defined, the `sim_com()` function executes the spatially explicit simulation
204 over discrete time steps. In each iteration, the model sequentially resolves dispersal and local
205 population dynamics. First, the effective carrying capacity ($K_{i,t}$) of every grid cell is dynamically
206 updated based on the local abundance of all interacting species (as defined by the interaction
207 matrix a). Populations then grow according to their intrinsic growth rates (r), constrained by these
208 dynamically updated realized niches. Simultaneously, individuals disperse across the landscape
209 according to species-specific kernels. This cycle repeats for the specified duration, generating a
210 complete spatiotemporal history of the metacommunity that captures the interplay between
211 environmental forcing, biotic interactions, and dispersal.

212 4.3. Observation and analysis

213 Following the simulation, users can analyse the "biological truth" directly or, optionally, pass the
214 results to the `virtual_ecologist()` function. This post-processing step applies the
215 observation constraints described in [Section 3.4](#) to the raw simulation output. By defining specific
216 sampling protocols (e.g., plot number, detection probability) at this stage, users generate an
217 "observed" dataset derived from the "true" state. This dual-output workflow allows researchers
218 to seamlessly benchmark analytical methods by comparing statistical inferences drawn from the
219 virtual samples against the known ground truth of the metacommunity. Following the simulation
220 (and optionally an observation process), the resulting community state can be analysed directly.
221 The package provides native plotting methods: `plot_series()` generates temporal

222 trajectories of total or mean abundance for all species, while `plot()` visualises the spatial
223 distribution (i.e. realised niches) of the metacommunity at specific time points.

224 5. Case studies

225 We present three case studies to validate the simulator against established ecological theory. The first
226 two examples benchmark `mrangr` against known biological patterns: the influence of dispersal on
227 biodiversity scaling and the dynamics of competition-colonization trade-offs. The third example
228 demonstrates the package's methodological utility, evaluating the limitations and potential of
229 inferring fundamental niches from observation-based data.

230 The three case studies were run in the same exemplary simulation environment, defined on a 20×20
231 grid (400 cells) with a 1 km resolution, assuming a coordinate system EPSG:2180. Trends in simulated
232 parameters were quantified and visualised using Generalized Additive Models for Location, Scale and
233 Shape (GAMLSS) to capture non-linear responses and heteroscedasticity.

234 5.1. Example 1: Testing the effect of dispersal on species diversity

235 Dispersal is the fundamental process connecting local communities, shaping biodiversity patterns at
236 multiple scales. In metacommunity theory, dispersal promotes local coexistence through the rescue
237 effect, yet potentially undermines regional diversity by homogenizing distinct communities (Mouquet
238 & Loreau, 2003). Consequently, the relationship between dispersal ability and diversity metrics is
239 expected to vary across scales. Increased dispersal should theoretically elevate local richness
240 (α -diversity) by overcoming dispersal limitation, while simultaneously eroding compositional turnover
241 (β -diversity) through mass effects. At the regional scale (γ -diversity), these opposing forces may
242 generate a unimodal response, where biodiversity peaks at intermediate dispersal rates that balance
243 colonization against competitive exclusion. Testing these predictions empirically is challenging due to
244 the difficulty of manipulating dispersal traits. Here, we demonstrate how `mrangr` can be used to

245 rigorously test these macroecological hypotheses by simulating metacommunities across a controlled
246 gradient of dispersal ranges while keeping niche requirements and interaction strengths constant.

247 In this example, the metacommunity consisted of 20 species. For each simulation replicate,
248 species-specific carrying capacity maps (K) were generated using spatially autocorrelated log-normal
249 distributions. Biotic interactions were modelled via an asymmetric interaction matrix (a) with
250 coefficients drawn from a normal distribution. The experimental gradient focused on dispersal ability.

251 We varied the mean dispersal distance from 100 m to 3000 m across 30 discrete intervals. Dispersal
252 was modelled using an exponential kernel, where the rate parameter is defined as $1/\text{mean}$ distance.

253 We performed 100 independent replicates for each dispersal scenario. Each simulation ran for 20 time
254 steps, sufficient to allow the metacommunity to reorganize from its initial state under the imposed
255 dispersal and interaction constraints. At the final time step, we calculated diversity metrics based on
256 Hill numbers with $q = 1$ (exponential of Shannon entropy):

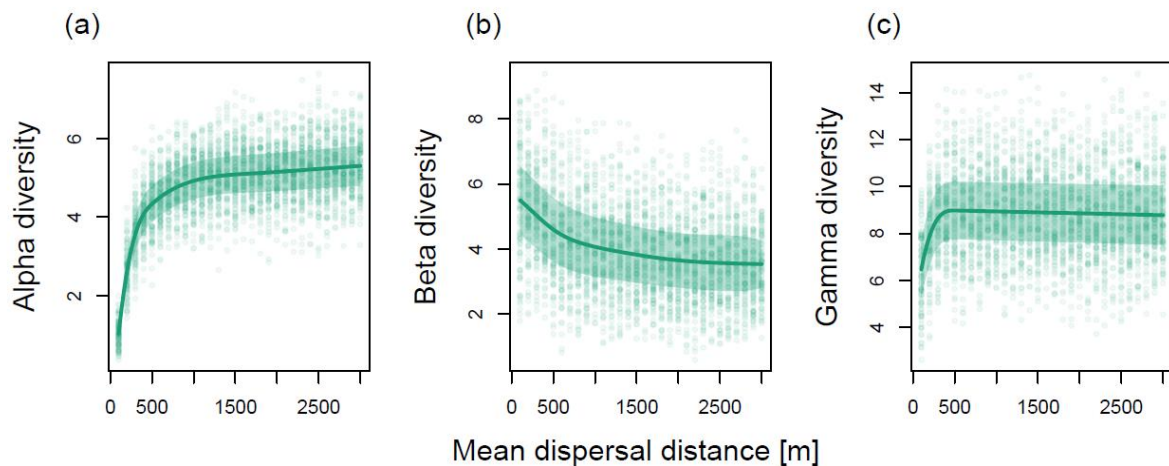
- 257 1. Alpha diversity (α): calculated as the mean local diversity across all 400 grid cells.
- 258 2. Gamma diversity (γ): calculated based on the total pooled abundance of each species across
259 the entire landscape.
- 260 3. Beta diversity (β): derived using additive partitioning: $\beta = \gamma - \alpha$.

261 The simulation results confirm the opposing effects of dispersal on biodiversity across spatial scales,
262 reproducing classic theoretical predictions (e.g., Mouquet & Loreau, 2003):

- 263 1. Local enrichment (α -diversity): As predicted, local species richness increased monotonically
264 with dispersal ability (Figure 2a). At low dispersal rates, local communities are impoverished
265 due to local extinctions and dispersal limitation. Increasing connectivity allows species to
266 colonize and persist in suboptimal patches ('sink' habitats) via the rescue effect, thereby
267 inflating local diversity.

268 2. Spatial homogenization (β -diversity): Conversely, compositional turnover declined sharply as
 269 dispersal increased (Figure 2b). High dispersal rates effectively mix the metacommunity,
 270 eroding the spatial distinctions driven by environmental heterogeneity.

271 3. The regional trade-off (γ -diversity): The response of regional diversity highlights the tension
 272 between local enrichment and spatial homogenization (Figure 2c). Gamma diversity increases
 273 rapidly at low dispersal distances as species overcome dispersal limitation, eventually
 274 saturating at a stable plateau. Unlike simple theoretical models that predict a decline in
 275 diversity at high dispersal rates due to global competitive exclusion, our results indicate that
 276 spatial heterogeneity in carrying capacity provides sufficient refuge for inferior competitors.
 277 In this high-dispersal regime, species sorting mechanisms allow species to efficiently track
 278 their environmental optima without being displaced from the landscape entirely, maintaining
 279 high regional diversity despite extensive mixing.



280

281 Figure 2. Response of metacommunity diversity components to mean dispersal distance. Scatterplots
 282 display (a) alpha, (b) beta, and (c) gamma diversity for metacommunities simulated with a regional
 283 pool of 20 species. Points represent individual simulation runs. Solid lines indicate the median and
 284 shaded regions represent the interquartile range, modelled using a Gaussian Location-Scale GAM
 285 (GAMLSS).

286 5.2. Example 2: Competition–colonization trade-off

287 A fundamental puzzle in community ecology is explaining how inferior competitors avoid exclusion in
288 landscapes dominated by superior species. The competition–colonization trade-off hypothesis
289 provides a classic metacommunity solution, proposing that species coexist by partitioning the
290 landscape based on dispersal ability rather than resource use (Tilman, 1994). In this framework,
291 inferior competitors persist as "fugitive species" by investing in superior colonization rates, allowing
292 them to occupy vacant patches before slower-dispersing dominants arrive to displace them.
293 Identifying this trade-off in empirical systems is often confounded by environmental heterogeneity
294 and complex trait correlations. In this example, we use `mrangr` to simulate a test of this hypothesis
295 by enforcing a strict constraint between competitive rank and dispersal distance, evaluating whether
296 this trade-off alone is sufficient to maintain regional coexistence in a spatially explicit context.

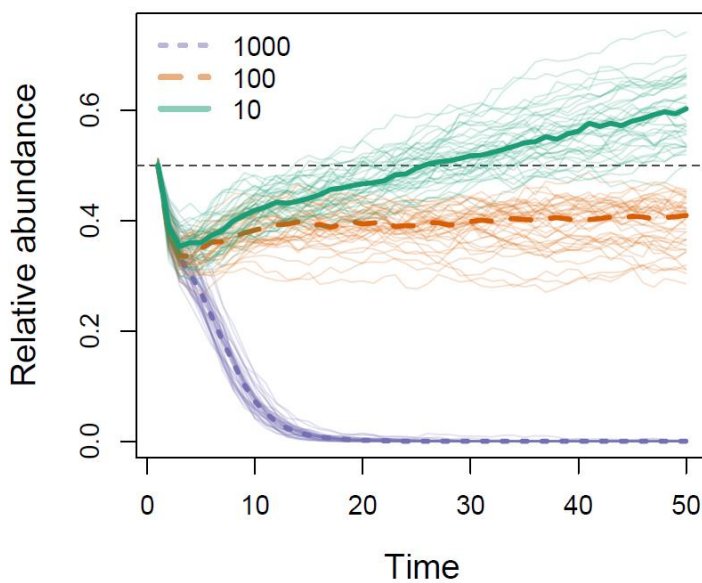
297 In this example, the metacommunity consisted of just two virtual species. To isolate the effect of
298 dispersal on coexistence, we controlled for environmental preferences by enforcing complete
299 fundamental niche overlap. Both species were assigned identical spatial habitat requirements,
300 differing only in their competitive fitness within that niche:

- 301 1. Species 1 (superior competitor): Assigned a baseline carrying capacity generated via a
302 log-normal distribution.
- 303 2. Species 2 (inferior competitor): Assigned a carrying capacity 20% lower than Species 1, across
304 the entire landscape.
- 305 3. Biotic interactions: We applied strong, symmetric competition between the species ($a = -1$).
306 Under these conditions — identical fundamental niches and distinct fitness levels — theory
307 predicts the deterministic exclusion of Species 2 by Species 1 in every grid cell.

308 We introduced a trade-off where the inferior competitor (Species 2) compensated for its lower fitness
309 with superior dispersal. We fixed the mean dispersal distance of Species 2 at 1000 m and
310 systematically varied the mean dispersal of the superior competitor (Species 1) across three scenarios:

- 311 1. No trade-off (Control): Species 1 also disperses 1000 m (equal dispersal, unequal fitness).
 312 2. Moderate trade-off: Species 1 disperses 100 m (10× disadvantage).
 313 3. Strong trade-off: Species 1 disperses 10 m (100× disadvantage).

314 We performed 40 independent replicates per scenario over 50 time steps. We tracked the relative
 315 abundance of the inferior competitor to evaluate whether spatial niche partitioning (via colonisation
 316 ability) could prevent exclusion despite the lack of niche differentiation.



317

318 Figure 3. Testing the competition-colonization trade-off. Temporal dynamics of the inferior
 319 competitor's relative abundance over 50 simulation steps. The inferior competitor (Species 2) has a
 320 fixed high dispersal distance (1000 m) but lower competitive fitness ($K_2 = 0.8 \times K_1$). Thin lines
 321 represent individual simulation trajectories ($n=40$), while thick lines indicate the median. Scenarios
 322 differ by the mean dispersal distance of the superior competitor (Species 1): 1000 m (violet, dotted
 323 line), 100 m (orange, dashed line), and 10 m (green, solid line).

324 The simulations demonstrate that dispersal advantage can effectively counteract competitive
 325 exclusion (Figure 3). In the absence of a trade-off, when both species shared equal dispersal
 326 capabilities (violet dotted line), the inferior competitor was rapidly driven toward extinction. However,

327 as the trade-off strength increased, the inferior competitor's persistence improved significantly. In the
328 strongest trade-off scenario (green solid line), where the superior competitor was severely dispersal-
329 limited (10 m), the inferior competitor successfully exploited vacant space, achieving numerical
330 dominance despite its lower fitness.

331 5.3. Example 3: Reconstruction of fundamental niches

332 Estimating the fundamental niche from field data is complicated by two filters: biotic interactions,
333 which constrain the realized distribution, and observational errors, which distort detection.
334 Consequently, ecological field data rarely reflect pure environmental potential (Soberón, 2007). Yet,
335 recovering this baseline is essential for forecasting species responses to novel environments. In this
336 example, we use `mrangr` to simulate a known ground truth and systematically evaluate whether
337 statistical models can penetrate these biological and observational layers to reliably reconstruct the
338 fundamental niche.

339 Spatially autocorrelated environmental variables were generated using Gaussian Random Fields via
340 the `K_sim()` function. The metacommunity consisted of 5 virtual species. For each species, the
341 fundamental niche (carrying capacity, K) was defined as a log-linear function of the environmental
342 covariates, ensuring a known ground truth for species-environment relationships. To model the
343 realized niche, we generated asymmetric interaction matrices (a) where off-diagonal elements were
344 drawn from a normal distribution $N(0, \delta^2)$. We systematically varied the interaction strength
345 parameter, δ , across a gradient to simulate metacommunities ranging from purely abiotic-driven ($\delta =$
346 0) to highly interactive systems ($\delta = 3$).

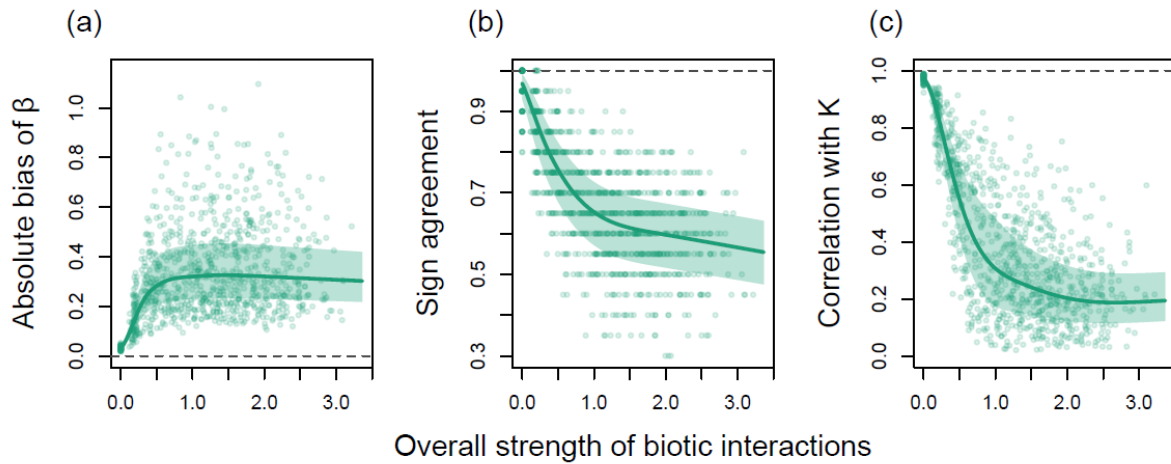
347 Simulations were initialized with abundances drawn from a Poisson distribution with expectations
348 equal to the local carrying capacity ($\lambda = K$). The system was evolved for 50 time steps, with the first
349 10 steps serving as a burn-in period to allow the community to reach a quasi-equilibrium state. To
350 replicate the spatiotemporal structure of empirical monitoring datasets, we employed the 'virtual
351 ecologist' module across the subsequent 40 time steps. We sampled 10% of the available site-time

352 combinations ($p_{\text{prop}} = 0.1$) and introduced observational error using a binomial distribution with
353 detection probability $p = 0.5$, mimicking the imperfect detection typical of wildlife surveys.

354 We attempted to reconstruct the fundamental niche from the sampled realized abundances using
355 Generalized Linear Mixed Models (GLMMs) fitted via the `glmmTMB` package. The models included the
356 true environmental covariates as predictors. We evaluated the performance of these reconstructions
357 against the true fundamental niche (K) using three metrics:

- 358 1. Bias of β : The absolute difference between the estimated environmental coefficient and the
359 true coefficient used to generate K .
- 360 2. Sign agreement: The proportion of simulations where the model correctly identified the
361 direction of the environmental response (positive/negative).
- 362 3. Correlation with K : The Spearman rank correlation between the spatially predicted
363 abundance surface and the true carrying capacity map.

364 Our simulations demonstrate that interaction strength substantially impairs the statistical recovery of
365 the fundamental niche. As the interaction strength increased, the spatial correlation between the
366 reconstructed niche and the true carrying capacity declined non-linearly, effectively uncoupling
367 realized abundance from environmental potential (Figure 4c). Concurrently, the absolute bias in
368 estimated environmental coefficients (β) rose (Figure 4a), indicating that biotic constraints
369 systematically distort the perceived magnitude of environmental preferences. Most critically, under
370 strong biotic regulation, the sign agreement dropped toward 0.5 (Figure 4b), equivalent to random
371 guessing. This implies that in highly interactive communities, standard correlative models frequently
372 misidentify positive environmental associations as negative (and vice versa), yielding spurious niche
373 estimates driven by community dynamics rather than abiotic suitability.



374

375 Figure 4. Influence of biotic interaction strength on the accuracy of fundamental niche estimation by
 376 the 'virtual ecologist'. Interaction strength is defined as the mean absolute value of off-diagonal
 377 elements in the interaction matrix. Estimation performance is evaluated via: (a) absolute bias of slope
 378 estimates (β); (b) sign agreement (proportion of estimated slopes matching the true sign); and
 379 (c) correlation between estimated abundances and true carrying capacity (K). Points represent
 380 individual metacommunities. Solid lines indicate the median and shaded regions represent the
 381 interquartile range, modelled using a Gaussian Location-Scale GAM (GAMLSS). Dashed horizontal lines
 382 indicate reference values for optimal performance (zero bias or perfect agreement/correlation).

383 6. Conclusions

384 The metacommunity concept has traditionally been framed within four major paradigms: species
 385 sorting, mass effects, patch dynamics, and neutral theory (M. A. Leibold et al., 2004). Recent work has
 386 shifted toward a unified process-based and prediction oriented framework (M. A. Leibold et al., 2022),
 387 yet operationalization of this synthesis and the ability to link observed patterns to underlying
 388 processes remains a key challenge (M. Leibold et al., 2025). Here, we address this issue by reducing
 389 metacommunity dynamics into three fundamental axes - space, time, and species - linked through
 390 core ecological processes.

391 Although this abstraction is necessarily simplified, `mrangr` captures both the biotic interactions that
392 drive local species coexistence, and the spatiotemporal population dynamics that determine
393 community assembly, while maintaining mechanistic flexibility. A central feature is the explicit
394 separation of the fundamental and realized niche, ensuring that realised co-distribution patterns
395 dynamically emerge from environmental potential and biotic processes parametrised as independent
396 inputs. By incorporating stochasticity across all processes, `mrangr` enables the generation of
397 parameter distributions from replicated simulations, facilitating robust statistical inference.

398 This provides a general and user-friendly framework to explore limits of inference, particularly the
399 identifiability of species interactions in metacommunity dynamics (Barbier et al., 2025). Furthermore,
400 being process-based, `mrangr` moves beyond null models, by enabling virtual experiments with
401 arbitrary biotic interaction structures, fully spatially explicit environments, and an integrated
402 observation process module. Therefore, it can serve as a platform for benchmarking of methods that
403 encompass metacommunity dynamics into species co-distribution patterns (Christopher D. Terry et
404 al., 2023; Morueta-Holme et al., 2016; Ovaskainen et al., 2017, 2019). This facilitates precise
405 mechanistic control over the primary processes driving community dynamics, allowing researchers to
406 replicate established patterns while exploring complex frontiers, such as the disentanglement of
407 abiotic filtering from competition, the interplay between niche and fitness differences, or the
408 spatiotemporal dynamics of species invasions.

409 7. Authors' contributions

410 KM and LK conceived the ideas and designed the methodology; KM and LK developed the algorithm;
411 KM led the software development and R package implementation; KM, MW, and LK wrote the
412 documentation and vignettes; MW contributed to the validation and testing of the software. All
413 authors contributed equally to the writing of the manuscript and gave final approval for publication.
414 LK acquired the funding and provided overall supervision for the project.

415 8. Funding Statement

416 The study was supported by the National Science Centre (NCN) in Poland (grant no.
417 2018/29/B/NZ8/00066). The computational resources supporting this work were provided by the
418 Poznań Supercomputing and Networking Centre (PCSS) (grant no. pl0090-01).

419 9. Conflict of interest statement

420 The authors declare no conflicts of interest.

421 10. Data availability statement

- 422 • The `mrangr` package is available on CRAN (<https://cran.r-project.org/package=mrangr>). It
423 comes with built-in function documentation and a vignette demonstrating its main
424 functionality and workflow logic.
- 425 • Contact details for issues with the package: <https://github.com/popecol/mrangr/issues>
- 426 • The package's source code can be accessed on GitHub (<https://github.com/popecol/mrangr>)
427 and Zenodo (<https://doi.org/10.5281/zenodo.18641951>).
- 428 • Package's website is hosted at <https://popecol.github.io/mrangr/>.
- 429 • The code and data used in the case studies are available on Zenodo
430 (<https://doi.org/10.5281/zenodo.18643290>).
- 431 • The preprint of this manuscript is available at:
432 <https://ecoevorxiv.org/repository/view/11808/>.

433 11. References

434 Adler, P. B., HilleRisLambers, J., & Levine, J. M. (2007). A niche for neutrality. *Ecology Letters*, *10*(2),
435 95–104. <https://doi.org/10.1111/j.1461-0248.2006.00996.x>

436 Araújo, M. B., & Rozenfeld, A. (2014). The geographic scaling of biotic interactions. *Ecography*, *37*(5),
437 406–415. <https://doi.org/10.1111/j.1600-0587.2013.00643.x>

438 Barbier, M., Bunin, G., & Leibold, M. A. (2025). Getting more by asking for less: Linking species
439 interactions to species co-distributions in metacommunities. *Peer Community Journal*, *5*.
440 <https://doi.org/10.24072/pcjournal.483>

441 Chesson, P. (2000). Mechanisms of Maintenance of Species Diversity. *Annual Review of Ecology and*
442 *Systematics*, *31*(1), 343–366. <https://doi.org/10.1146/annurev.ecolsys.31.1.343>

443 Christopher D. Terry, J., Langdon, W., & Rossberg, A. G. (2023). Codistribution as an indicator of
444 whole metacommunity response to environmental change. *Ecography*, *2023*(7), e06605.
445 <https://doi.org/10.1111/ecog.06605>

446 Dallas, T. (2014). metacom: An R package for the analysis of metacommunity structure. *Ecography*,
447 *37*(4), 402–405. <https://doi.org/10.1111/j.1600-0587.2013.00695.x>

448 Fallert, S., Li, L., & Cabral, J. S. (2025). metaRange: A framework to build mechanistic range models.
449 *Methods in Ecology and Evolution*, *16*(1), 49–56. <https://doi.org/10.1111/2041-210X.14461>

450 Hagen, O., Flück, B., Fopp, F., Cabral, J. S., Hartig, F., Pontarp, M., Rangel, T. F., & Pellissier, L. (2021).
451 gen3sis: A general engine for eco-evolutionary simulations of the processes that shape
452 Earth's biodiversity. *PLOS Biology*, *19*(7), e3001340.
453 <https://doi.org/10.1371/journal.pbio.3001340>

454 Hijmans, R. J. (2026). *terra: Spatial Data Analysis* (Version R package version 1.8-94) [Computer
455 software]. <https://rspatial.org/>

456 Ke, P.-J., & Letten, A. D. (2018). Coexistence theory and the frequency-dependence of priority
457 effects. *Nature Ecology & Evolution*, *2*(11), 1691–1695. [https://doi.org/10.1038/s41559-018-](https://doi.org/10.1038/s41559-018-0679-z)
458 [0679-z](https://doi.org/10.1038/s41559-018-0679-z)

459 Leibold, M. A., Chase, J. M., & Ernest, S. K. M. (2017). Community assembly and the functioning of
460 ecosystems: How metacommunity processes alter ecosystems attributes. *Ecology*, *98*(4),
461 909–919. <https://doi.org/10.1002/ecy.1697>

462 Leibold, M. A., Holyoak, M., Mouquet, N., Amarasekare, P., Chase, J. M., Hoopes, M. F., Holt, R. D.,
463 Shurin, J. B., Law, R., Tilman, D., Loreau, M., & Gonzalez, A. (2004). The metacommunity
464 concept: A framework for multi-scale community ecology. *Ecology Letters*, 7(7), 601–613.
465 <https://doi.org/10.1111/j.1461-0248.2004.00608.x>

466 Leibold, M. A., Rudolph, F. J., Blanchet, F. G., De Meester, L., Gravel, D., Hartig, F., Peres-Neto, P.,
467 Shoemaker, L., & Chase, J. M. (2022). The internal structure of metacommunities. *Oikos*,
468 2022(1), oik.08618. <https://doi.org/10.1111/oik.08618>

469 Leibold, M., Barbier, M., Bittleston, L., Clark, A. T., Cuellar-Gempeler, C., D’Andrea, R., Frans, V. F.,
470 Khattar, G., Miller, Z., Peres-Neto, P. R., & Wisnoski, N. I. (2025). *Linking Pattern to Process in*
471 *Metacommunities: Challenges and Opportunities*.
472 <https://ecoevortexiv.org/repository/view/9021/>

473 Lin, J.-H., Quan, Y.-J., & Han, B.-P. (2024). MetaIBM: A Python-based library for individual-based
474 modelling of eco-evolutionary dynamics in spatial-explicit metacommunities. *Ecological*
475 *Modelling*, 492, 110730. <https://doi.org/10.1016/j.ecolmodel.2024.110730>

476 Malinowska, K., Markowska, K., & Kuczyński, L. (2023). Making virtual species less virtual by reverse
477 engineering of spatiotemporal ecological models. *Methods in Ecology and Evolution*, 14(9),
478 2376–2389. <https://doi.org/10.1111/2041-210X.14176>

479 Markowska, K., Malinowska, K., & Kuczyński, L. (2025). rangr: An R package for mechanistic, spatially
480 explicit simulation of species range dynamics. *Methods in Ecology and Evolution*, 16(3), 468–
481 476. <https://doi.org/10.1111/2041-210X.14475>

482 Meynard, C. N., Leroy, B., & Kaplan, D. M. (2019). Testing methods in species distribution modelling
483 using virtual species: What have we learnt and what are we missing? *Ecography*, 42(12),
484 2021–2036. <https://doi.org/10.1111/ecog.04385>

485 Morueta-Holme, N., Blonder, B., Sandel, B., McGill, B. J., Peet, R. K., Ott, J. E., Violle, C., Enquist, B. J.,
486 Jørgensen, P. M., & Svenning, J. (2016). A network approach for inferring species

487 associations from co-occurrence data. *Ecography*, 39(12), 1139–1150.
488 <https://doi.org/10.1111/ecog.01892>

489 Mouquet, N., & Loreau, M. (2003). Community Patterns in Source-Sink Metacommunities. *The*
490 *American Naturalist*, 162(5), 544–557. <https://doi.org/10.1086/378857>

491 Ovaskainen, O., Rybicki, J., & Abrego, N. (2019). What can observational data reveal about
492 metacommunity processes? *Ecography*, 42(11), 1877–1886.
493 <https://doi.org/10.1111/ecog.04444>

494 Ovaskainen, O., Tikhonov, G., Norberg, A., Guillaume Blanchet, F., Duan, L., Dunson, D., Roslin, T., &
495 Abrego, N. (2017). How to make more out of community data? A conceptual framework and
496 its implementation as models and software. *Ecology Letters*, 20(5), 561–576.
497 <https://doi.org/10.1111/ele.12757>

498 Soberón, J. (2007). Grinnellian and Eltonian niches and geographic distributions of species. *Ecology*
499 *Letters*, 10(12), 1115–1123. <https://doi.org/10.1111/j.1461-0248.2007.01107.x>

500 Thompson, P. L., Guzman, L. M., De Meester, L., Horváth, Z., Ptacnik, R., Vanschoenwinkel, B., Viana,
501 D. S., & Chase, J. M. (2020). A process-based metacommunity framework linking local and
502 regional scale community ecology. *Ecology Letters*, 23(9), 1314–1329.
503 <https://doi.org/10.1111/ele.13568>

504 Tilman, D. (1994). Competition and Biodiversity in Spatially Structured Habitats. *Ecology*, 75(1), 2–16.
505 <https://doi.org/10.2307/1939377>

506 Vellend, M. (2016). *The Theory of Ecological Communities*. Princeton University Press.
507 <https://doi.org/10.1515/9781400883790>

508 Zurell, D., Berger, U., Cabral, J. S., Jeltsch, F., Meynard, C. N., Münkemüller, T., Nehrbass, N., Pagel, J.,
509 Reineking, B., Schröder, B., & Grimm, V. (2010). The virtual ecologist approach: Simulating
510 data and observers. *Oikos*, 119(4), 622–635. [https://doi.org/10.1111/j.1600-](https://doi.org/10.1111/j.1600-0706.2009.18284.x)
511 [0706.2009.18284.x](https://doi.org/10.1111/j.1600-0706.2009.18284.x)

512